Numerical and experimental investigations of the formation process of ferrofluid droplets

Jing Liu • Say-Hwa Tan • Yit Fatt Yap• Min Yuan Ng • Nam-Trung Nguyen

J. Liu · S.-H. Tan · M. Y. Ng · N.-T. Nguyen (✉)

School of Mechanical and Aerospace Engineering,

Nanyang Technological University, 50 Nanyang Avenue, Singapore 639798, Singapore

e-mail: mntnguyen@ntu.edu.sg

Present Address:
S.-H. Tan
Max Planck Institute for Dynamics and Self-Organization, 37073 Göttingen, Germany

Y. F. Yap
Department of Mechanical Engineering, The Petroleum Institute, P.O. Box 2533, Abu Dhabi, UAE

Abstract

This paper reports both experimental and numerical investigations of the formation process of ferrofluid droplets in a flow focusing configuration with and without an applied magnetic field. In the experiment, the homogenous magnetic field was generated using an electromagnet. The magnetic field in the flow direction affects the formation process and changes the size of the droplets. The change in the droplet size depends on the magnetic field strength and the flow rates. A numerical model was used to investigate the force balance during the droplet breakup process. A linearly magnetizable fluid was assumed. Particle level set method was employed to capture the interface movement between the continuous fluid and the dispersed fluid. Results of the droplet formation process and the flow field are discussed for both cases with and without the magnetic field. Finally, experimental and numerical results are compared.

Keywords Ferrofluid· Magnetic field· Flow focusing· Microfluidics

1 Introduction

Magnetic particles inside a droplet allow its control and manipulation using a magnetic field (Pamme 2006). Magnetic beads with a size ranging from one to tens of micrometers are not homogenously distributed in the droplet, and can easily cluster or be extracted from the liquid under a strong magnetic field (Long et al. 2009; Lehmann et al. 2006; Tsuchiya et al. 2008; Shikida et al. 2006). Magnetic particles such as magnetite (Fe_3O_4) with a few nanometers in

size can avoid the above problem of the larger magnetic beads. Fluids with smaller homogenously suspended magnetic particles are called ferrofluids and behave like liquid magnets in a magnetic field. A surfactant is added into the fluids to prevent the agglomeration of the particles induced from the magnetic dipole interaction and sedimentation due to the gravity of the particles (Rosensweig 1985; Odenbach 2003). Ferrofluids can display various interesting behaviors and patterns under the different strengths of the magnetic field. Moreover, the fluid exhibits a decrease in viscosity under an applied AC magnetic field (Zahn 2001).

Ferrofluid droplets suspended in another immiscible fluid form an emulsion. For instance, an emulsion of water-based ferrofluid in oil can be formed in a T-junction microchannel (Tan et al. 2010). Ferrofluid droplets and emulsions have a variety of applications in biology and engineering such as detection of defects in ferromagnetic components (Philip et al. 1999), cell sorting (Zborowski et al. 1999; Kose et al. 2009), optical filter (Philip et al. 2003), PCR (Sun et al. 2007), pump and valve (Hartshorne et al. 2004). In addition, ferrofluid emulsion was used as shadow mask for micro-fabrication to prevent chemical and UV exposure by varying the pattern of magnetic field (Yellen et al. 2004). Ferrofluid droplets can be used for magnetic manipulation as well (Friedman and Yellen 2005.

Ferrofluid droplets can be manipulated by employing planar electromagnets (Nguyen et al. 2006). Ferrofluid plugs driven by a permanent magnet can be used as a liquid piston for fluid transport in a polymerase chain reactor (Sun et al. 2008). Recently, Nguyen et al. (2010) studied the effect of magnetowetting on a sessile ferrofluid droplet by employing a moving magnet. The effects of the magnetic field strength, base diameter of the droplet, and the moving speed of the magnet were investigated. The formation process of ferrofluid droplets at a microfluidic T-junction can be controlled by the position of an external permanent magnet (Tan et al. 2010).

Other than magnetic field, additional energy sources such as heat, electric field, and laser were also widely employed to actuate droplets. Under an applied electric field, droplet manipulation is based on the electrostatic force (Link et al. 2006). The droplet behavior can be changed by localized heating from a single or line patterns laser. A single laser spot can increase the formed droplet volume in a cross flowing channel, and switch the droplet transport path at a bifurcation due to laser heating (Baroud et al. 2007a, b). The interfacial film dynamics during droplets adhesion because of laser heating was studied by Dixit et al. (2010). However, varying droplets size by employing magnetic field was not reported by other research groups. In addition, magnetic manipulation can be carried out with a permanent magnet without electric power.

The numerical models provide a tool to further explain the behaviors of ferrofluid droplet, the interaction between capillarity and ferrohydrodynamics, and how the magnetic force affects the droplet formation. The numerical treatment of the present problem can be extended to other multi-phase multi-physics problems in microfluidics. The mathematical formulation for hydrodynamics of ferrofluid was discussed by Rosensweig (1985). The deformation of a freely suspended droplet and a sessile droplet in a uniform magnetic field was previously numerically studied by coupling the magnetic field, the free surface, and the fluid flow (Lavrova et al. 2006; Sero-Guillaume et al. 1992). The stable shape is determined by the interaction between

magnetic force and the interfacial tension force. The shape will jump to an elongated one within a certain threshold of magnetic field (Bacri and Salin 1982). To study the dynamics of a freely suspended droplet, an analytical model was built to explain the oscillation caused by the perturbing magnetic field (Potts et al. 2001). A ferrofluid droplet falling down in a non-magnetic fluid was modeled by Korlie et al. (2008). A linearly magnetizable fluid was considered in this model. Afkhami et al. (2008) studied the equilibrium state of a hydrophobic ferrofluid droplet under a uniform magnetic field numerically and experimentally (Afkhami et al. 2008). A non-linear magnetic fluid and the volume of fluid (VOF) method were used to model the multiphase flow. The magnetic potential was governed by a linear equation in an axial symmetric cylindrical coordinates.

The main challenge in modeling multiphase systems is describing the interface movement (Liu and Nguyen 2010). There are different techniques to predict the interface location such as level set method (LSM) and VOF. The algorithm of LSM for tracking the moving interface on the fixed-grid system was demonstrated by Osher and Sethian (1988). The level set function, $\phi(\vec{x}, t)$, was introduced over the whole domain or near the interface and was defined as a signed shortest normal distance from the interface. A review of VOF method was given by Scardovelli and Zaleski (1999). The volume fraction function was introduced and defined in a volume fraction field throughout the whole computational domain.

This paper reports both experimental and numerical investigation of the formation process of ferrofluid droplets under a uniform magnetic field. Water-based ferrofluid and silicone oil, respectively, worked as the dispersed and the continuous fluids in a flow focusing microchannel. A uniform magnetic field generated by an electromagnet was used to control the formation process. The numerical model assumes the ferrofluid to be a linear magnetic material. Particle LSM was used to calculate the movement of the interface between ferrofluid and silicone oil. Both experiment and simulation show the same effect of the magnetic field on the size of the droplets formed. Detailed hydrodynamic analysis during the formation process was carried out for both cases with and without the magnetic field.

2 Experimental methods

2.1 Design and fabrication of the test device

A flow focusing configuration was employed to form the ferrofuid droplets. The test device has a size of 10 mm × 10 mm. Figure 1a shows the layout of the device. Port one guides the continuous fluid to flow into two equal branches with the same flow rate. The two branches act as two side channels of the flow focusing configuration. Port two is used to introduce the dispersed fluid into the main channel. Figure 1b shows the geometry of the flow focusing junction where the droplets are formed. The microchannels have a square cross section of 100 μm × 100 μm. Without the applied magnetic field, ferrofluid droplets were formed in the squeezing regime. The test device was fabricated using standard soft lithography (Liu et al. 2009). The polydimethylsiloxane (PDMS) substrate was peeled off from the master mold and bonded to a glass slice with a spin coated PDMS layer of 200-μm thickness using oxygen plasma treatment (790 Series, Plasma-Therm, Inc., FL, USA). The device was then aligned to the electromagnet so that the magnetic field is parallel to the main channel, Fig. 1b.

2.2 Materials

In the experiment, water-based ferrofluid (Ferrotech, EMG 807) works as the dispersed phase. At 27°C, the dynamic viscosity and density are μ_d = 2 mPa s and ρ_d = 1100 kg m^{-3}, respectively. The subscript "d" refers to the dispersed phase. The particles volume concentration is 1.8% and the beginning susceptibility is χ = 0.39. The magnetization of this ferrofluid was described in the previous work of Tan et al. (2010). Silicone oil (Sigma-Aldrich, 378364) works as the continuous phase. The dynamic viscosity and density are μ_c = 96 mPa s and ρ_c = 960 kg/m^3, respectively. The subscript 'c' refers to the continuous phase. The interfacial tension between the ferrofluid and the oil is 12 mN m^{-1}.

2.3 Experimental setup

To generate a uniform magnetic field, a coil with 350 turns was spiraled round a 'U' shape steel core with a small air gap of 26 mm as shown in the inset of Fig. 2. A DC power source (Instek, GPS-3030DD) was used to vary the magnitude of the magnetic field strength. The magnetic flux densities at different current intervals were measured using a commercial gaussmeter with an accuracy of 1% (Hirst, GM05, UK). The current of the electromagnet was varied from 0 to 3 A at an interval of 0.5 A. The corresponding magnetic flux density varies from 0 to 40 mT (Fig. 2). The ferrofluid behaves as a non-linear magnetizable material because of the strong magnetic field (Tan et al. 2010). The fluids were delivered to the device by two separate precision syringe pumps (KD Scientific Inc., USA).

In the experiment, the flow rate of silicone oil varied from Q_c = 20 μl/h to 24 μl/h. The flow rates ratio of the continuous and dispersed phases were fixed at four. Ferrofluid droplets were imaged with a high speed camera (Photron, APX RS) using a ×10 objective lens on a Nikon (TE2000) inverted fluorescence microscope. Images were acquired at a rate of 1000 frames per second.

3 Numerical simulation

3.1 Problem description

The numerical simulation was carried out with a three-dimensional (3D) model. The dimensions of flow focusing structure are the same as those of the experimental device depicted in Fig. 1b. The velocities of silicone oil and ferrofluid at the inlet were assumed to be fully developed with the mean velocities $\bar{u}_c$ and $\bar{U}_d$ for the continuous and disperse fluids, respectively

$$\bar{u}_c = \frac{Q_c}{2WH}, \bar{v}_d = \frac{Q_d}{WH} \tag{1}$$

where W and H are the is width and height of the microchannel. No-slip boundary condition is applied to the walls. Outflow boundary condition is used at the outlet. Only one quarter of the domain was calculated due to the symmetry of the channel geometry and the flow field.

Symmetry boundary conditions are applied at the symmetry surfaces. The actual densities and viscosities of the liquids were used. Following dimensionless numbers were used for the characterization of the formation process:

$$\mathrm{Ca} = \frac{\mu_c u_c}{\sigma}, Re = \frac{\rho_c u_c L}{\mu_c}, \chi_m, B_m = \frac{\mu_0 L H^2}{\sigma} \mu^* = \frac{\mu_c}{\mu_d}, \quad \rho^* = \frac{\rho_c}{\rho_d}, u^* = \frac{u_c}{u_d}, t^* = \frac{t u_c}{L} \tag{2}$$

where σ is the interfacial tension, L is characteristic length as well as the width of the channel inlet as shown in Fig. 1, and t is the time. The values of the capillary number (Ca) and the Reynolds number (Re) are less than unity. The magnetic bond number (B_m) describes the ratio between the magnetic force and the interfacial tension force. At a fixed interfacial tension, the magnetic bond number (B_m) represents the strength of the field. The susceptibility (χ_m) is the property representing the response of the ferrofluid to an applied magnetic field.

3.2 Governing equations

The magnetic field is described by the Maxwell equations for nonconducting fluids (Rosensweig 1985)

$$\vec{\nabla} \times \vec{H} = 0 \tag{3}$$

$$\vec{\nabla} \cdot \vec{B} = 0 \tag{4}$$

where $\vec{H}$ and $\vec{B}$ are the magnetic field strength and the magnetic flux density. Considering a ferrofluid domain, Ω_d, surrounded by a nonmagnetizable medium, Ω_c, both $\vec{B}$ and $\vec{H}$ satisfy

$$\vec{B} = \begin{cases} \mu_0(\vec{H} + \vec{M}), & \text{if } \Omega_d \\ \mu_0(\vec{H}), & \text{if } \Omega_c \end{cases} \tag{5}$$

$\mu_0 = 4\pi \times 10^{-7}$ N/A^2 is the permeability of the free space, $\vec{M}$ is the magnetization of the ferrofluid. In our model, the magnetization of the ferrrofluid is assumed to be a linear function of the magnetic field strength

$$\vec{M} = \chi_m \vec{H}, \tag{6}$$

where χ_m is the susceptibility of the ferrofluid. The magnetic permeability of the ferrofluid is defined as $\mu_1 = \mu_0 (1+ \chi_m)$. Thus, the flux density inside the ferrofluid is $\vec{B} = \mu_1 \vec{H}$.

Introducing the magnetic scalar potential ψ in the form of $\vec{H} = -\nabla\psi$ to satisfy Eq. 3 and Eq. 4 yields

$$\nabla \cdot [(1 + \chi_{\mathrm{m}})\nabla\psi] = 0. \tag{7}$$

The permeability abruptly changes across the interface between two immiscible phases. Thus, the scalar potential, ψ, changes as the interface moves. The magnetic susceptibility can be solved within the whole computational domain based on the harmonic mean

$$\frac{1}{1+\chi_m} = \frac{1-H}{1+\chi_c} + \frac{H}{1+\chi_d}. \tag{8}$$

The magnetic force is given by Rosensweig (1985)

$$\vec{F}_{\mathrm{m}} = -\frac{1}{2}\mu_0\left|\vec{H}\right|^2\nabla\chi_{\mathrm{m}}, \tag{9}$$

where $\nabla\chi_{\mathrm{m}} = \frac{\mathrm{d}_{\chi_m}}{\mathrm{d}_\phi}\nabla\phi$ and

$$\frac{\mathrm{d}_{\chi_m}}{\mathrm{d}_\phi} = \frac{(1+\chi_{\mathrm{d}})(1+\chi_{\mathrm{c}})(\chi_{\mathrm{d}}-\chi_{\mathrm{c}})D(\phi)}{\left[(1+\chi_{\mathrm{d}}) + H(\chi_{\mathrm{c}}-\chi_{\mathrm{d}})\right]^2}. \tag{10}$$

where ∅ is level set function (Yap et al. 2006). The value is the shortest normal distance to the interface. D(∅) is the delta function that is zero everywhere except near the interface, and its definition is

$$D(\phi) = \begin{cases} \frac{1+\cos(\pi\phi/\varepsilon)}{2\varepsilon} & |(\phi)| < \varepsilon \\ 0 & \text{otherwise} \end{cases} \tag{11}$$

The magnetic force only acts on the interface where the discontinuity in magnetic permeability takes place and will vanish if the permeability is constant. The boundary condition of the magnetic field satisfies

$$\vec{H}\cdot\hat{n} = -\frac{\partial\psi}{\partial n}, \quad \forall\vec{x}\in\partial\Omega. \tag{12}$$

The incompressible Navier–Stokes equations are used to solve the flow field of both continuous and dispersed phases

$$\begin{aligned}\frac{\partial}{\partial t}(\rho\vec{u}) + \nabla\cdot(\rho\vec{u}\vec{u}) = &-\nabla p + \nabla\cdot\left[\mu\left(\nabla\vec{u} + \nabla\vec{u}^T\right)\right] \\ &+ \vec{F}_{\mathrm{s}} + \vec{F}_{\mathrm{m}},\end{aligned} \tag{13}$$

where $\vec{F}$ is the interfacial tension force (Yap et al. 2006)

$$\vec{F}_s = -\sigma\kappa\hat{n}_f D(\phi), \tag{14}$$

where κ is the curvature, and $\hat{n}_f$ is the normal vector to the interface. The gravity is neglected in this model. An incompressible and unsteady media is assumed

$$\frac{\partial\rho}{\partial t} + \nabla\cdot(\rho\vec{u}) = 0. \tag{15}$$

The jumps of the properties ρ and μ near the interface were smoothed with Heaviside function in the whole computational domain (Yap et al. 2006).

The N–S Eq. 13, continuum Eq. 15, and magnetic potential Eq. 7 are solved on a Cartesian staggered grid using finite volume method. The velocity field and the pressure field are coupled by the SIMPLER algorithm (Patankar 1980). The combined convection–diffusion effect is predicted by the second-order accurate total variation diminishing (TVD) discretization schemes. The time integration used a fully implicit scheme. A particle LSM is employed to capture the motion of interface between two immiscible phases (Ho et al. 2009). The calculation of interfacial tension uses the continuous surface force model (Brackbill 1992).

3.3 Grid independent study

Validation and grid refinement were first carried out. As a case study, the mean velocities of the main channel and the lateral channel are set as $\bar{u}_c$ = 0.0025m/s and $\bar{U}_d$ = 0.01 m/s. Both fluids have same densities and viscosities of $\rho_c = \rho_d$ = 1000 kg m^{-3}and $\mu_c = \mu_d$ = 1 mPas. The interfacial tension is set as σ= 1 mN m^{-1}. The results of our numerical scheme are compared with the VOF method of the commercial code Fluent. Table 1 shows a good agreement for the normalized droplet volumes $V^* = V_d/L^3$. Since our numerical scheme uses the staggered grid to approach the actual geometry while the VOF method can define the real geometry, the error can be reduced with further grid refinement. The grid size of 184 × 62 × 26 will be used in the subsequent simulation.

4 Results and discussion

The formation process of the ferroffluid droplets in the absence of the magnetic field was first investigated. Both simulated and measured evolutions of the formed droplet are shown in Fig. 3. The discrepancy occurs after the droplet breakup at t = 187 ms marked with a circle (Fig. 3a, t = 187 ms, 207 ms). The tip of the ferrofluid is sharper in the experimental results possibly because of change in geometry caused by swelling of the device material (PDMS) when exposed to silicone oil (Venkatraman et al. 1994; Lee et al. 2003).

The force caused by the viscous stress acting on the interface is proportional to the tip area

and the velocity gradient. Together with the pressure, the viscous force provides a squeezing action on the tip to move it downstream. Acting in the opposite direction, the interfacial tension keeps the ferrofluid tip from moving forward. As shown in Fig. 3, at the beginning of the formation process (t = 0, 47 ms), the curvature of the tip is bigger and results in a larger capillary force, which is proportional to the curvature and the interfacial tension. The pressure increases as the dispersed phase blocks the throat, which together with the viscous stress stretches the ferrofluid tip to move forward. Therefore, the ferrofluid thread becomes thinner and its circumference reduces until the thinner thread can no longer hold back the ferrofluid tip (t = 173 ms). At the moment of breakup, the new tip and the formed droplet move oppositely upstream and downstream due to the higher pressure inside the ferrofluid (t = 187 ms).

Figure 4 shows the simulated instantaneous streamlines during the droplet formation process from the early stage to the breakup without the magnetic effect. The streamlines describe the direction of fluid flow over time. As shown in Fig. 4, from t = 47 ms to t = 116 ms, the flow directions are changed and two counter rotating vortices near the wall appear inside the throat. Several pairs of vortices distribute along the interface of the thread at t = 166 ms. It is interesting to see that two pairs of the vortices grow bigger when the thread is ready to breakup at t = 173 ms.

After recording the images with the high-speed camera, we measured the droplet diameter using a customized MATLAB program. For each data point, a total of 20 droplets were measured. However, as the resultant droplet has an apparent diameter bigger than the depth of the channel, it assumes a discoid shape (Nie et al. 2008). Hence, the measured result slightly overestimates the actual droplet diameter. The image sequences of the droplet formation were processed using another customized MATLAB program. The interface between the ferrofluid and the oil was detected. The time-evolving image was constructed by the individual interface images and serves as a visualization tool for the droplet formation process. Figure 5 shows the evolution of the droplet formation process in the presence of the magnetic field. The ferrofluid tips were elongated, and the formed droplet size is big compared to the case without the magnetic field shown in Fig. 3. In the experiment, the time to form a droplet is about 1.016 s when the magnetic flux density is B = 42.3 mT. This time is almost twice the time needed for the case without the magnetic field of 0.592 s.

Figure 6 depicts the simulated magnetic scalar potential ψ over time with B_m = 0.3, χ_d = 5 as in the case of the simulation (Fig. 5b). The corresponding numerical velocity field is depicted in Fig. 7. It takes much longer for the ferrofluid droplet to complete the formation process. The streamlines of droplet forming become different under a magnetic field as described in Fig. 7. In this situation, the magnetic force acts as a drag force on the interface of the ferrofluid tip. The growing tip results into the increase of the number of the vortices.

A flow in opposite direction occurs at t = 86.3 ms (Fig. 7). The interaction of the magnetic force and the capillary force leads to an elongated tip. The elongation is more serious at a large magnetic force, F_m. As a result, the tip does not exhibit the spherical shape as in the case without the magnetic field. The magnitude of the velocities increases gradually until the breakup happens. These phenomena are different from the case without the magnetic field.

The pressure outside the thread increases slowly. The curvature of the thread is small and changes slowly because of the high pressure inside the thread. Finally, a bigger droplet is formed when the interfacial tension force cannot withhold the ferrofluid. The formed droplet has the shape of an ellipsoid due to the stretching effect of the magnetic force (t = 489.2 ms to 546.8 ms in Fig. 7). The relationship between the normalized diameter (D^*) and the magnetic Bond number (B_m) is shown in Fig. 8. The discrepancy in the curves of the numerical and the experimental results are caused by the different responses of the magnetization to the applied magnetic field strength.

The ferrofluid is assumed to be a linear magnetic material in the numerical models while it behaves as a non-linear magnetic material in the experiment. A non-linear model would be more accurate to obtain a quantitative comparison with the experiment results. However, the aim of the present numerical study is the qualitative understanding of the behavior of the ferrofluid under an applied magnetic field and of the magnetic-hydrodynamic interactions. The present results provide the theoretical basis for further development of more comprehensive and accurate models describing the actual physics of the problem. Nevertheless, both results show the similar trends, and they obviously indicate the two regions affected by the flow rates.

A higher flow rate can form a relatively larger droplet in regime I of Fig. 8, and smaller droplet in region II of Fig. 8. Figure 9 shows the states of the ferrofluid tips just before the breakup in the two regimes. In regime I, the diameter of tip is smaller than the channel width. In regime II, the blockage happens in the case of Q_c = 20 µl/h, Q_d = 5 µl/h, and $\eta \ll W$. The pressure difference and the shear stress can increase dramatically. The size of the formed droplet is more sensitive to the applied magnetic force at lower flow rates. The same phenomenon was also observed for the formation process at a T-junction (Tan et al. 2010).

5 Conclusions

In conclusion, this paper reports the behavior of the formation process of ferrofluid droplets in a flow focusing configuration. The effect of an applied magnetic field on the droplet size and the velocity field was investigated experimentally and numerically. The size of droplet increases with increasing magnetic field strength. The sensitivity of the droplet size on the magnetic field depends on the flow rates of both continuous and the dispersed fluids. Although the ferrofluid behaves as a non-linear magnetizable material in the experiment and a linear magnetizable relationship was assumed in the numerical model, similar trends were obtained. The relationship of the magnetic bond number and the normalized droplet diameter was discussed. The higher the magnetic bond number, the larger is the volume of the formed droplet.

In the absence of the magnetic field, a couple of opposite flow appears in the flow focusing channel as results of the interaction between the pressure drop, viscous drag force, and interfacial tension. The pressure drop and the viscous drag force push the ferrofluid forward while the interfacial tension keeps the tip backward. In the presence of a magnetic field, the ferrofluid tip is pulled forward due the additional magnetic force. The thread and the tip become longer resulting in a longer formation time. The hydrodynamics arising in the formation process of a ferrofluid droplet was further investigated with the help of a

numerical model. Two cases of with and without magnetic field was analyzed. The results presented in this paper show that using an external homogenous magnetic field is an alternative to control the droplet size of a ferrofluid emulsion.

References

Afkhami S, Renardy Y, Renardy M, Riffle JS, St Perre T (2008) Field-induced motion of ferrofluid droplets through immiscible viscous media. J Fluid Mech 610:363–380

Afkhami S, Tyler AJ, Renardy Y, Renardy M, St. Pierre TG, Woodward RC, Riffle JS (2010) Deformation of a hydrophobic ferrofluid droplet suspended in a viscous medium under uniform magnetic fields. J Fluid Mech 1–27

Bacri JC, Salin D (1982) Instability of ferrofluid magnetic drops under magnetic field. J Phys (Paris) Lett V 43:649–654

Baroud CN, Delville JP, Gallaire F,Wunenburger R (2007a) Thermocapillary valve for droplet production and sorting. Phys Rev E 75(4)

Baroud CN, Robert De Saint Vincent M, Delville JP (2007b) An optical toolbox for total control of droplet microfluidics. Lab Chip 7(8):1029–1033

Brackbill JU (1992) A continuum method for modeling surface tension. J Comput Phys 100(2):335–354

Dixit SS, Kim H, Vasilyev A, Eid A, Faris GW (2010) Light-driven formation and rupture of droplet bilayers. Langmuir 26(9): 6193–6200

Friedman G, Yellen B (2005) Magnetic separation, manipulation and assembly of solid phase in fluids. Curr Opin Colloid Interface Sci 10:158–166

Hartshorne H, Backhouse CJ, Lee WE (2004) Ferrofluid-based microchip pump and valve. Sens Actuators 99:592–600

Ho PC, Yap YF, Nguyen NT, Chai JC, Wong TN, Yobas L (2009) Thermally mediated droplet formation at a microfluidic T-junction. ASME ICNMM2009-82056

Korlie MS, Mukherjee A, Nita BG, Stevens JG, Trubatch AD, Yecko P (2008) Modeling bubbles and droplets in magnetic fluids. J Phys Condens Matter 20:204153

Kose AR, Fischer B, Mao L, Koser H (2009) Label-free cellular manipulation and sorting via biocompatible ferrofluids. Proc Natl Acad Sci USA 106:21478–21483

Lavrova O, Matthies G, Mitkova T, Polevikov V, Tobiska L (2006) Numerical treatment of free surface problems inferrohydrodynamics. J Phys Condens Matter 218(38):S2657–S2669

Lee JN, Park C, Whitesides GM (2003) Solvent compatibility of poly(dimethylsiloxane)-based microfluidic devices. Anal Chem 75(23):6544–6554

Lehmann U, Hadjidj S, Parashar VK, Vandevyver C, Rida A, Gijs MAM (2006) Two-dimensional magnetic manipulation of microdroplets on a chip as a platform for bioanalytical applications. Sens Actuators B 117(2):457–463

Link DR, Grasland-Mongrain E, Duri A, Sarrazin F, Cheng ZD, Cristobal G, Marquez M, Weitz DA (2006) Electric control of droplets in microfluidic devices. Angew Chem Int Ed 45(16): 2556–2560

Liu J, Nguyen NT (2010) Numerical simulation of droplet-based microfluidics—a review. Micro Nanosyst 2(3):193–201

Liu J, Yap YF, Nguyen NT (2009) Behavior of microdroplets in diffuser/nozzle structures. Microfluid Nanofluid 6(6):835–846

Long Z, Shetty AM, Solomon MJ, Larson RG (2009) Fundamentals of magnet-actuated droplet manipulation on an open hydrophobic surface. Lab Chip 9(11):1567–1575

Nguyen NT, Ng KM, Huang X (2006) Manipulation of ferrofluid droplets using planar coils. Appl Phys Lett 89(5):052509

Nguyen NT, Zhu G, Chua YC, Phan VN, Tan SH (2010) Magnetowetting and sliding motion

of a sessile ferrofluid droplet in the presence of a permanent magnet. Langmuir 26(15):12553–12559
Nie Z, Seo M, Xu S, Lewis PC, Mok M, Kumacheva E, Whitesides GM, Garstecki P, Stone HA (2008) Emulsification in a microfluidic flow-focusing device: effect of the viscosities of the liquids. Microfluid Nanofluid 5(5):585–594
Odenbach S (2003) Ferrofluids—magnetically controlled suspensions. Colloids Surf 217:171–178
Osher S, sethian JA (1988) Fronts propagating with curvature-dependent speed: algorithms based on Hamilton-Jaacobi formulations. J Comput Phys 79(1):12–49
Pamme N (2006) Magnetism and microfluidics. Lab Chip 6(1):24–38
Patankar SV (1980) Numerical heat transfer and fluid flow. Hemisphere, New York
Philip J, Rao CB, Raj B, Jayakumar T (1999) An optical technique for the detection of surface defects in ferromagnetic samples. Meas Sci Technol 10(6):N71–N75
Philip J, Jaykumar T, Kalyanasundaram P, Raj B (2003) A tunable optical filter. Meas Sci Technol 14:1289–1294
Potts HE, Barrett RK, Diver DA (2001) Dynamics of freely-suspended drops. J Phys D 34(17):2529–2536
Rosensweig RE (1985) Ferrohydrodynamics. Cambridge University Press, London
Scardovelli R, Zaleski S (1999) Direct numerical simulation of free-surface and interfacial flow. Annu Rev Fluid Mech 31:567–603
Sero-Guillaume OE, Zouaoui D, Bernardin D, Brancher JP (1992) The shape of a magnetic liquid drop. J Fluid Mech 241:215–232
Shikida M, Takayanagi K, Inouchi K, Honda H, Sato K (2006) Using wettability and interfacial tension to handle droplets of magnetic beads in a micro-chemical-analysis system. Sens Actuators B 113(1):563–569
Sun Y, Kwok YC, Nguyen NT (2007) A novel circular ferro-fluid driven flow-through microchip for rapid DNA amplification. 383–386
Sun Y, Nguyen NT, Yien CK (2008) High-throughput polymerase chain reaction in parallel circular loops using magnetic actuation. Anal Chem 80(15):6127–6130
Tan SH, Nguyen NT, Yobas L, Kang TG (2010) Formation and manipulation of ferrofluid droplets at a microfluidic T-junction. J Micromech Microeng 20(4):045004
Tsuchiya H, Okochi M, Nagao N, Shikida M, Honda H (2008) On-chip polymerase chain reaction microdevice employing a magnetic droplet-manipulation system. Sens Actuators B 130(2): 583–588
Venkatraman S, Nixon A, Highe A (1994) Deformation behavior of poly(dimethyl siloxane) networks. II. Equilibrium swelling. J Appl Polym Sci 52(11):1619–1627
Yap YF, Chai JC, Wong TN, Toh KC, Zhang HY (2006) A global mass correction scheme for the level-set method. Numer Heat Transfer B 50(5):455–472
Yellen BB, Fridman G, Friedman G (2004) Ferrofluid lithography. Nanotechnology 15:S562–S565
Zahn M (2001) Magnetic fluid and nanoparticle applications to nanotechnology. J Nanopart Res 3:73–78
Zborowski M, Sun L, Moore LR, Stephen Williams P, Chalmers JJ (1999) Continuous cell separation using novel magnetic quadrupole flow sorter. J Magn Magn Mater 194:224–230

List of Tables

List of Figures

VOF			LSM			Difference (%)
Cell number	Δt	V^*	Cell number	Δt	V^*	
14280	2E−5	0.3127	93 × 32 × 14	2E−5	0.28038	10.3
68663	1E−5	0.29986	116 × 40 × 17	2E−5	0.28656	4.4
117560	5E−6	0.29633	184 × 62 × 26	1E−5	0.28828	2.7

Table 1

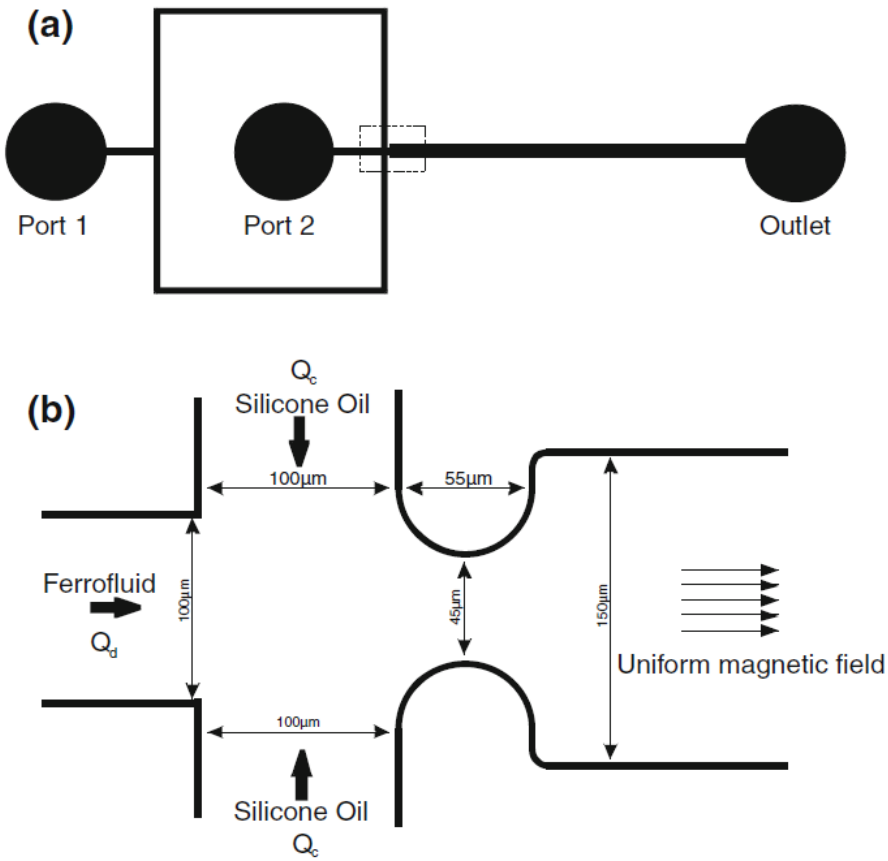
(a)
Port 1
Port 2
Outlet
(b)
Q_c
Silicone Oil
100µm
55µm
Ferrofluid
Q_d
100µm
45µm
150µm
Uniform magnetic field
100µm
Silicone Oil
Q_c

Fig. 1

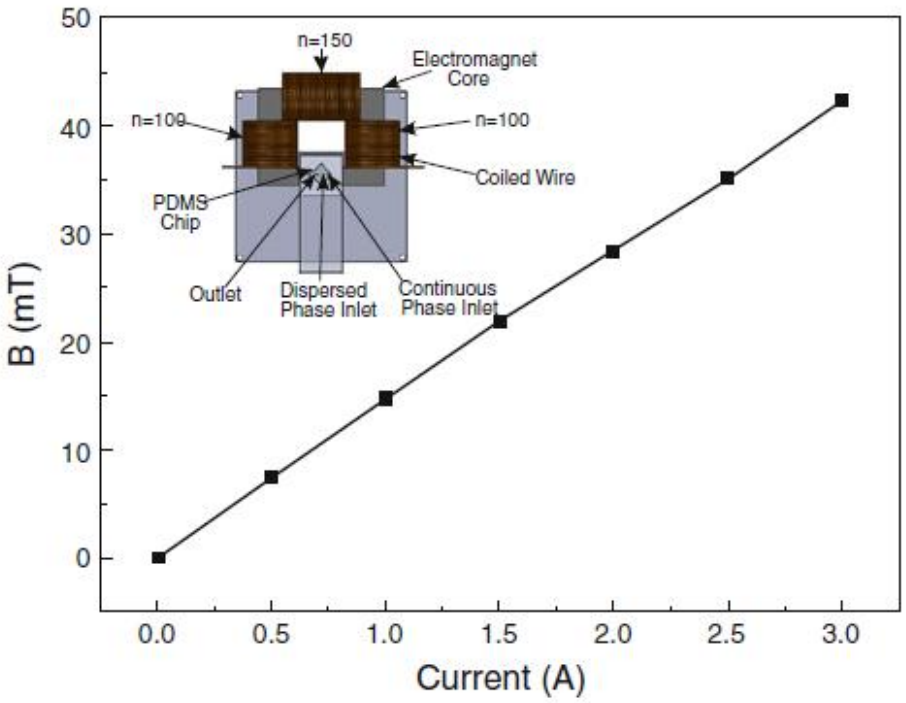
n=150
Electromagnet
Core
n=109
n=100
Coiled Wire
PDMS
Chip
Outlet
Dispersed
Phase Inlet
Continuous
Phase Inlet
B (mT)
Current (A)
0
10
20
30
40
50
0.0
0.5
1.0
1.5
2.0
2.5
3.0

Fig. 2

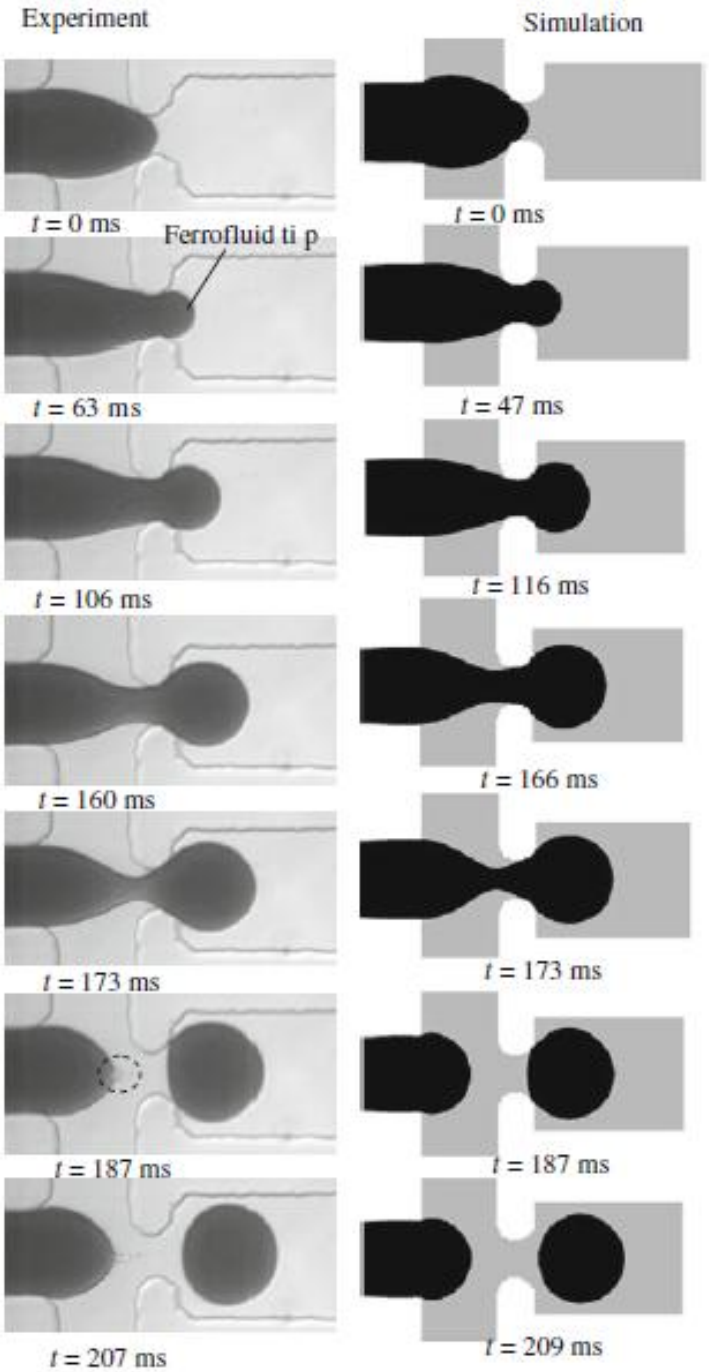
Experiment
Simulation
t = 0 ms
Ferrofluid ti ρ
t = 0 ms
t = 63 ms
t = 47 ms
t = 106 ms
t = 116 ms
t = 160 ms
t = 166 ms
t = 173 ms
t = 173 ms
t = 187 ms
t = 187 ms
t = 207 ms
t = 209 ms

Fig. 3

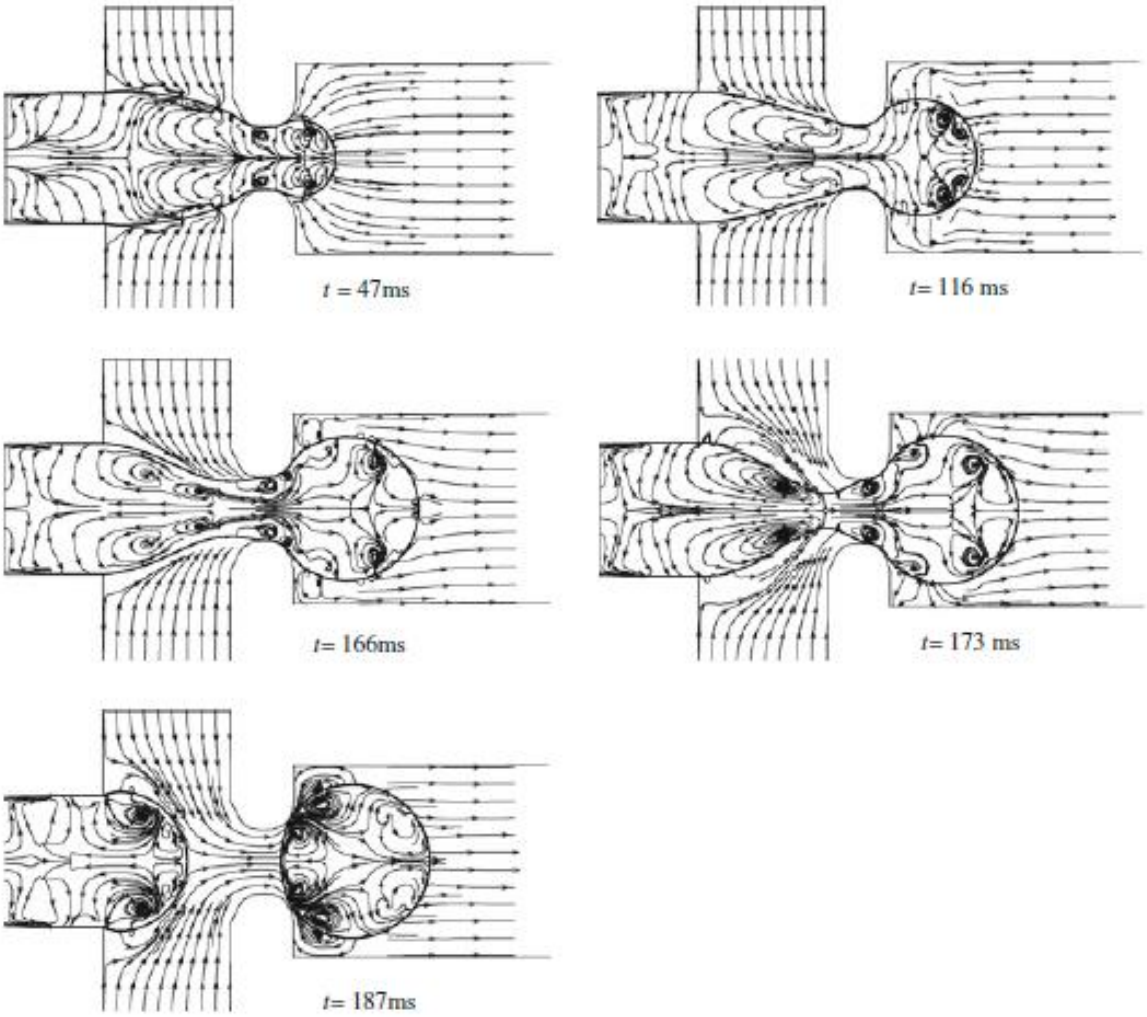

Fig.4

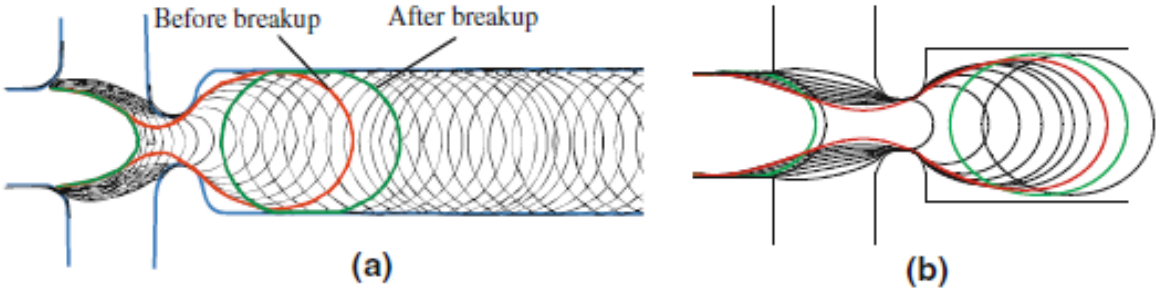

Fig. 5

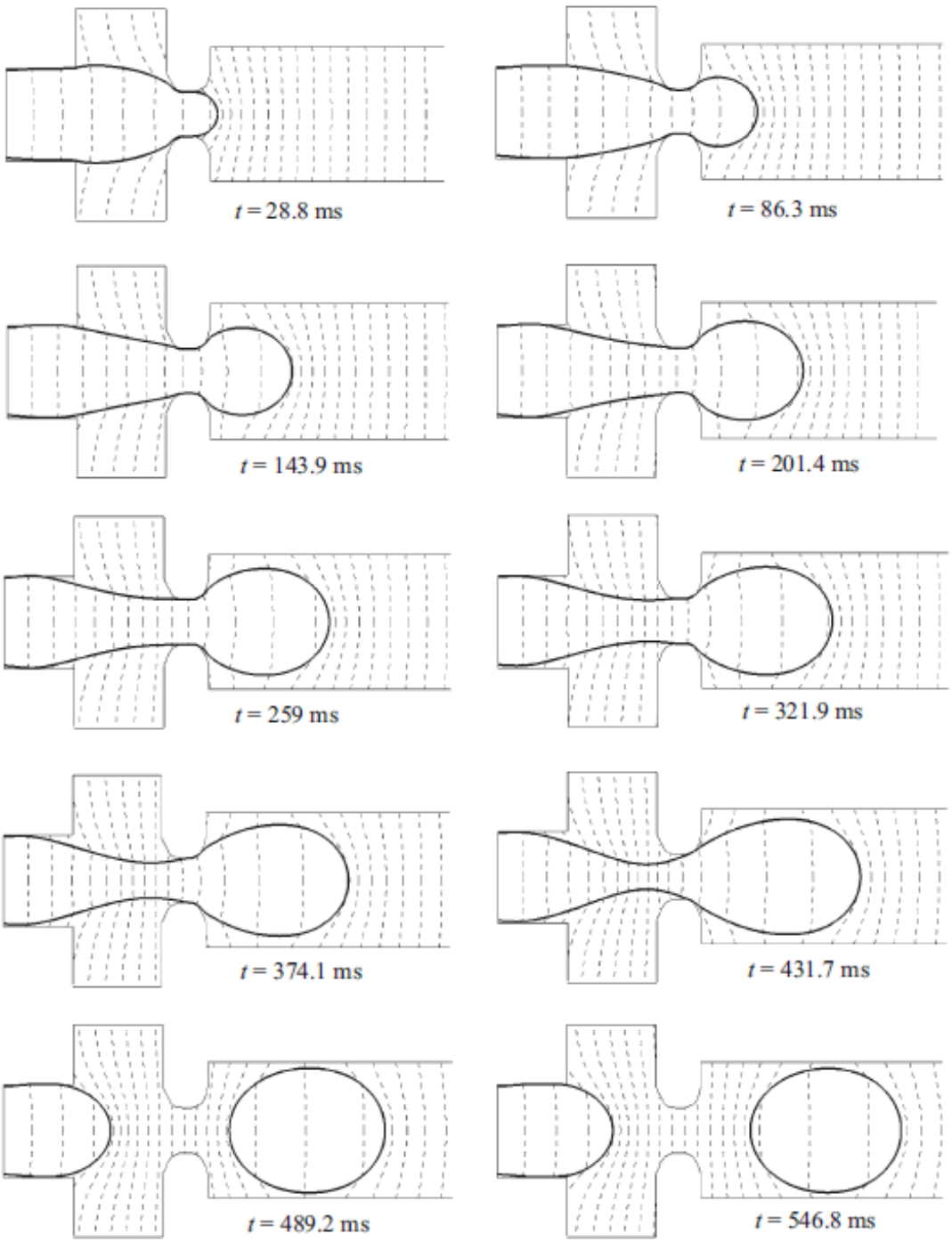
t = 28.8 ms
t = 86.3 ms
t = 143.9 ms
t = 201.4 ms
t = 259 ms
t = 321.9 ms
t = 374.1 ms
t = 431.7 ms
t = 489.2 ms
t = 546.8 ms

Fig. 6

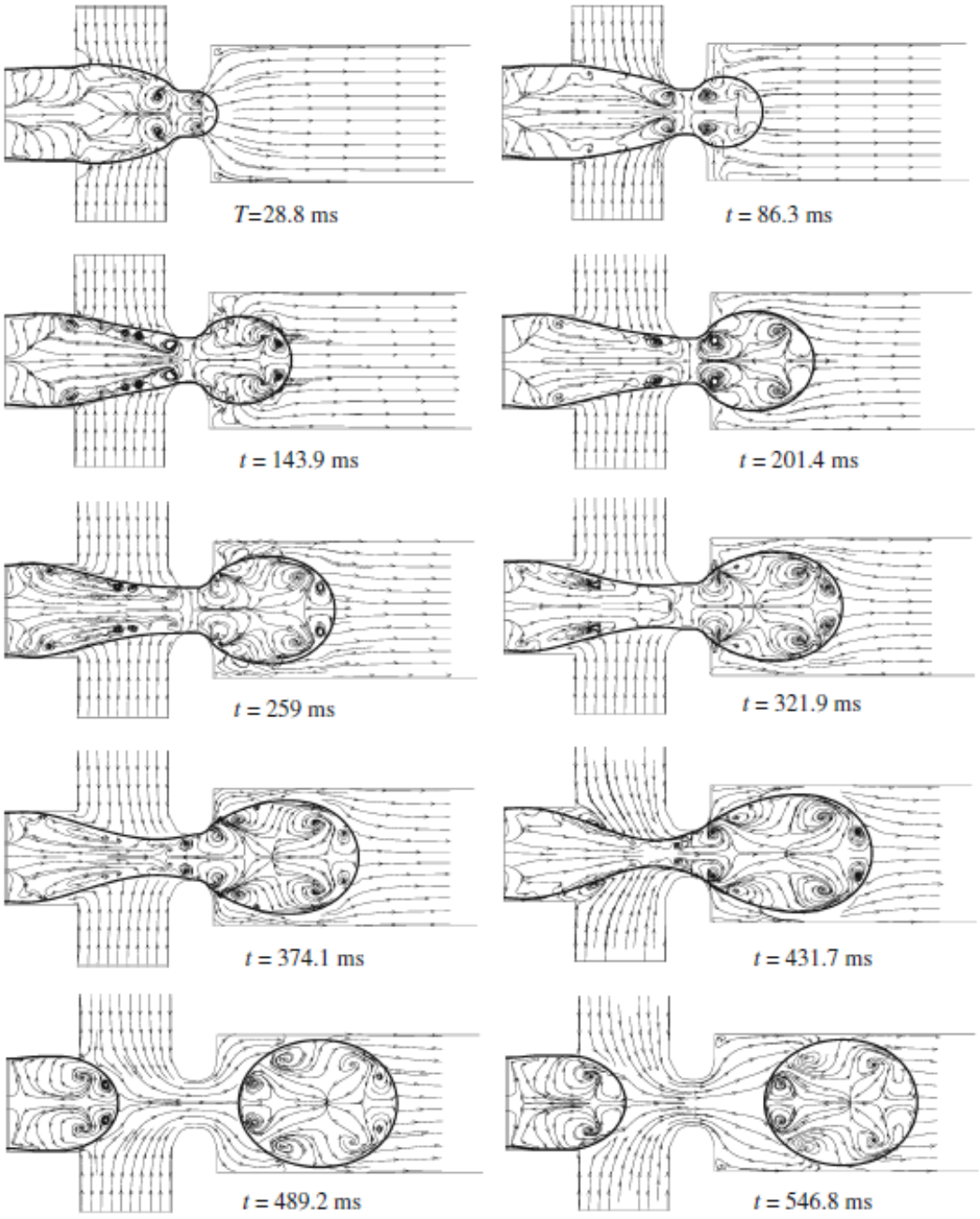
T=28.8 ms
t = 86.3 ms
t = 143.9 ms
t = 201.4 ms
t = 259 ms
t = 321.9 ms
t = 374.1 ms
t = 431.7 ms
t = 489.2 ms
t = 546.8 ms

Fig. 7

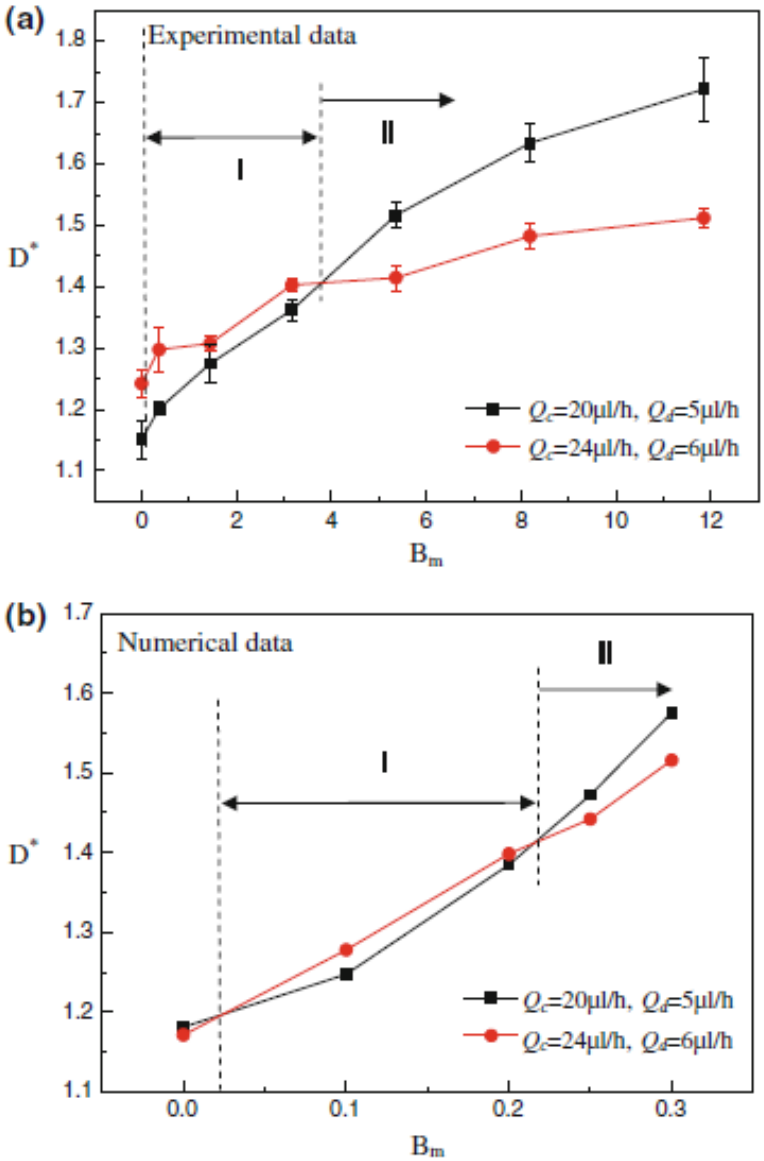
(a)
Experimental data
I
II
D*
Bm
Qc=20μl/h, Qd=5μl/h
Qc=24μl/h, Qd=6μl/h
(b)
Numerical data
I
II
D*
Bm
Qc=20μl/h, Qd=5μl/h
Qc=24μl/h, Qd=6μl/h

Fig. 8

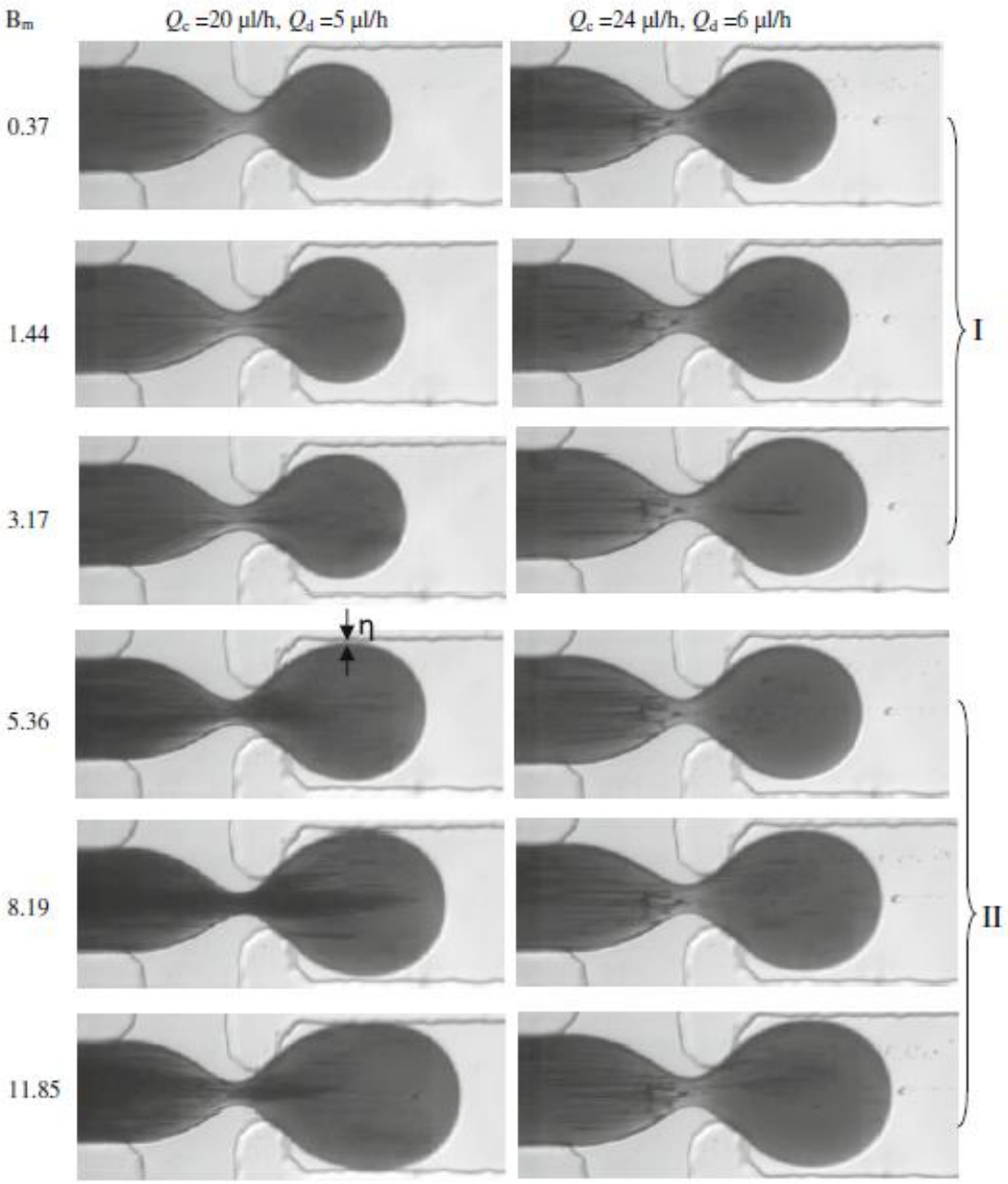
B_m
Q_c =20 μl/h, Q_d =5 μl/h
Q_c =24 μl/h, Q_d =6 μl/h
0.37
1.44
3.17
5.36
8.19
11.85
η
I
II

Fig. 9